Energy Conversion and Management 66 (2013) 165–172

Contents lists available at SciVerse ScienceDirect

Energy Conversion and Management

journal homepage: www.elsevier.com/locate/enconman

Designing high efficiency segmented thermoelectric generators

Constantinos Hadjistassou [a,b,*], Elias Kyriakides [a,b], Julius Georgiou [a,b,c]

[a] KIOS Research Center for Intelligent Systems and Networks, 132 Kyrineias Avenue, Aglantzia, 2113 Nicosia, Cyprus
[b] Department of Electrical and Computer Engineering, University of Cyprus, 75 Kallipoleos Street, PO Box 20537, 1678 Nicosia, Cyprus
[c] Holistic Electronics Research Lab, 75 Kallipoleos Street, PO Box 20537, 1678 Nicosia, Cyprus

ARTICLE INFO

Article history:
Received 9 January 2012
Received in revised form 2 July 2012
Accepted 3 July 2012
Available online 23 November 2012

Keywords:
Analytical model
Computational model
Efficiency
Segmented
Temperature
Thermoelectric generator

ABSTRACT

Improving the efficiency of thermoelectric devices is critical to their widespread adoption. Here a design methodology, formulated on computational and analytical modeling, derives the optimum efficiency and geometry of segmented Bi_2Te_3–PbTe Thermoelectric Generators (TEGs) between ≈298 K and ≈623 K ($\Delta T \approx 325$ K). Comparisons between the different TEG designs, in terms of the electrical load to TEG electrical resistance ratio ($m = R_L/R_{TEG}$), are simplified thanks to the devised maximum efficiency to temperature gradient ($\beta_{max} = \eta/\Delta T$) metric. Quasi-computational results of β_{max} show that the collective Seebeck coefficient Bi_2Te_3–PbTe ($\tilde{\alpha}$) design sustains a higher electrical load in relation to the homogeneous Bi_2Te_3 and PbTe materials. The average ($\bar{\alpha}$) and collective ($\tilde{\alpha}$) Seebeck coefficient Bi_2Te_3–PbTe configurations, in comparison to Bi_2Te_3 and PbTe, exhibit a considerably higher (60–68%) source and sink thermal resistance matching ($\Theta_{TEG} = \Theta_{Hx}$). The proposed segmented Bi_2Te_3–PbTe ($\tilde{\alpha}$) TEG yields a peak efficiency of 5.29% for a ΔT of 324.6 K.

1. Introduction

Photovoltaics and concentrated solar power currently dominate the renewable solar power generation landscape. In meeting the prevailing and imminent energy demands of the world, given the comparative advantages of each technology, it will be critical to diversify the power generation mix with the integration in the building and transportation sectors of other solar energy conversion technologies. Enhanced efficiency and reduced cost thermoelectrics (TE), which directly convert thermal energy into electricity, are poised to make significant contributions towards this direction.

Thermoelectric (or Seebeck) devices are solid state electric generators with no moving parts. Semiconductor materials, with TE properties, when subject to a temperature gradient across their ends produce an electromotive force (emf). Efficient TE materials are characterized by a high thermoelectric figure of merit (≈1): $z \cdot T$, where $z = ((\alpha^2\sigma)/\kappa)$, T is the absolute temperature (K), α the Seebeck coefficient, σ the electrical conductivity, and κ the thermal conductivity. Advantages such as the high degree of reliability, simplicity, tacit operation, lack of vibrations, and scalability render Thermoelectric Generators (TEGs) ideal for small scale, distributed power generation, and energy harvesting applications [1].

According to the *compatibility factor*, herein denoted by

$$\dot{s} = \left(\sqrt{1 + z \cdot T} - 1\right)/(\alpha T) \tag{1}$$

the efficiency of segmented TEG (STEG) materials increases when the two joined TE materials are compatible, that is, their $\dot{s}$ values do not differ by a factor of two or more [2]. Application of the compatibility factor to *segmented* and *cascaded* TEG designs showed that the use of incompatible TE materials results in a drop in efficiency [3].

Progress in sophisticated nanoscale TE materials as well as strategies to enhance their thermopower and reduce their thermal conductivity have been outlined by Snyder et al. [4]. Other investigators, using computational tools and a prototype model, have examined the influence of the heat exchangers' thermal resistance on the TEG efficiency [5]. Depending on the particular circumstances, the application of TEGs on vehicles for heat recovery resulted in unfavorable and beneficial results [6]. More recently, a flat-panel solar thermoelectric generator device, incorporating high-performance nanostructured TE materials and spectrally-selective solar absorbers, in an evacuated environment, with a demonstrated maximum efficiency of 4.6% has been proposed [7].

One of the most effective ways to boost the efficiency of a thermoelectric generator is to establish a large temperature gradient (ΔT) across the TEG constituent elements. In applications other than thermal energy waste recovery, concentrated solar energy, using relatively inexpensive optics (e.g., Fresnel lens), can help create a large temperature differential across a TEG. Noticeably, even with a high

* Corresponding author at: KIOS Research Center for Intelligent Systems and Networks, 132 Kyrineias Avenue, Aglantzia, 2113 Nicosia, Cyprus. Tel.: +357 99198151; fax: +357 22893455.
E-mail addresses: chatzis@ucy.ac.cy (C. Hadjistassou), elias@ucy.ac.cy (E. Kyriakides), julio@ucy.ac.cy (J. Georgiou).

0196-8904/$ - see front matter © 2012 Elsevier Ltd. All rights reserved.
http://dx.doi.org/10.1016/j.enconman.2012.07.030

Nomenclature

$A_{i,j}$	cross-sectional area of *p*- and *n*-type TEG thermoelements (m^2)
E	electric field ($N\,C^{-1}$)
h_0	total enthalpy ($m^{-2}\,s^{-1}$)
I	electric current (A)
J_{max}	maximum current density ($A\,m^{-2}$)
ℓ	length of the TEG elements (m)
$m = \frac{R_L}{R_{TEG}}$	electrical load resistance to TEG electrical resistance ratio
$n = \frac{\Theta_{TEG}}{\Theta_{Hx}}$	TEG to heat sink and heat source thermal resistance ratio
n_{TEG}	number of thermoelement pairs
p	static pressure ($N\,m^{-2}$)
R_L	electrical load resistance (Ω)
R_{TEG}	TEG electrical resistance (Ω)
T_C	heat sink temperature (K)
T_H	heat source temperature (K)
T_{Inter}	Bi_2Te_3–PbTe interface temperature (K)
$\overline{T}_{Inter}$	average Bi_2Te_3–PbTe interface temperature (K)
z	material thermoelectric figure of merit (K^{-1})
Z	device thermoelectric figure of merit (K^{-1})

Greek letters

α	thermoelectric material Seebeck coefficient ($V\,K^{-1}$)
$\bar{\alpha}$	average TE material Seebeck coefficient ($V\,K^{-1}$)
$\tilde{\alpha}$	collective TE material Seebeck coefficient ($V\,K^{-1}$)
$\beta = \frac{\eta}{\Delta T}$	efficiency to temperature gradient ratio (K^{-1})
$\bar{\eta}$	average Bi_2Te_3–PbTe Seebeck coefficient efficiency
$\tilde{\eta}$	collective Bi_2Te_3–PbTe Seebeck coefficient efficiency
Θ_{Hx}	heat sink and heat source thermal resistance ($K\,W^{-1}$)
Θ_{TEG}	TEG thermal resistance ($K\,W^{-1}$)
κ	thermal conductivity ($W\,m^{-1}\,K^{-1}$)
Λ	thermal conductance ($W\,K^{-1}$)
μ	dynamic viscosity ($kg\,m^{-1}\,s^{-1}$)
ρ	electrical resistivity ($\Omega\,m$)
ρ_m	mass-density ($kg\,m^{-3}$)
σ	electrical conductivity ($\Omega^{-1}\,m^{-1}$)
$\tau_{\imath\jmath}$	viscous stress in the $\jmath$ and $\imath$-directions, respectively ($N\,m^{-2}$)
ϕ	electric potential ($J\,C^{-1}$)

temperature difference, the performance of a TEG varies appreciably, largely, due to α, σ, and κ being temperature dependent.

In circumventing the latter limitation two or more TE materials can be joined in series to form a segmented TEG. The rationale behind the STEG design is to boost the overall TEG system efficiency by having individual TEG segments operating at their optimum (or near-optimum) $z \cdot T$ within the corresponding operating temperature range. Augmented TEG efficiencies have been recently realized at the experimental level [8] including designs for space applications [9].

Here a design methodology is proposed, based upon computational and analytical modeling, of a STEG with a heat sink (cold) temperature (T_C) of 298.2 K and a heat source (high) temperature (T_H) of 622.8 K (ΔT = 324.6 K). The efficiency of bismuth telluride (Bi_2Te_3), lead (II) telluride (PbTe), and the average ($\bar{\alpha}$) and collective ($\tilde{\alpha}$) Seebeck coefficient segmented Bi_2Te_3–PbTe configurations are determined as a function of the electrical load resistance to the TEG electrical resistance ($m = R_L/R_{TEG}$) ratio and the TEG and heat source and sink thermal resistance matching ($\Theta_{TEG} = \Theta_{Hx}$).

The segmented Bi_2Te_3 ($\tilde{\alpha}$) system overestimates the maximum efficiency to temperature gradient ratio ($\beta_{max} = \eta/\Delta T$) while Bi_2Te_3–PbTe ($\tilde{\alpha}$) yields a β_{max} value which resides intermediate to the β_{max} values of Bi_2Te_3 and PbTe. Technically, it is possible to develop the preceding temperature gradient of $\Delta T \approx 325$ K using inexpensive Fresnel lens, at a concentration factor $CF \approx 50$, where CF is the ratio of the optically active collector area to the absorber area upon which solar radiation impinges. The application of concentrator solar optics, which serves to emphasize such a possibility, has been extensively covered elsewhere [10]. This paper focuses on the application of segmented TE materials as facilitated by solar thermal energy.

2. Segmented TEGs

Considering the behavior of the figure of merit ($z \cdot T$) for TE materials, as a function of the operational temperature range of 622.8 K and 298.2 K, it is evident that: (a) no single material is thermally stable within the entire temperature regime [11] and (b) higher overall performance can be realized if two (or more) TE materials are utilized for each thermoelement [12]. In the low temperature range, Bi_2Te_3 was selected due to its high figure of merit whereas PbTe, due to its thermal stability, is more suitable for the top temperature regime. Other combinations of materials can also be used, if desired. Unless, the gain in system performance is justified by the use of more than two TE materials, connected in series, undue structural complexity due to material discontinuities – resulting also in higher manufacturing costs – is something to be avoided.

In ascertaining the merits and shortcomings of various design configurations, different theoretical scenarios were investigated

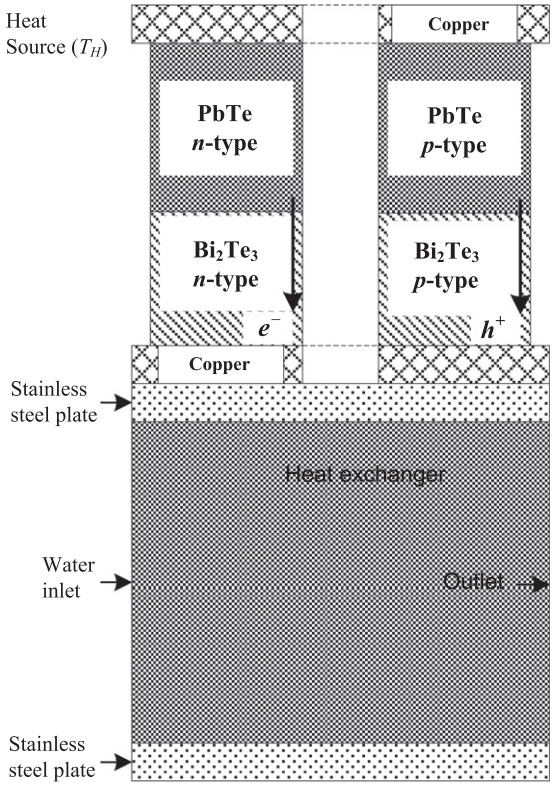

Fig. 1. Schematic of the proposed segmented bismuth telluride-lead telluride TEG with an active cooling heat exchanger (figure not to scale).

Table 1
Lead telluride (PbTe) TE material particulars.

Parameter	Value (units)	Reference
Peak TEG power (W_{mp})	5 W	–
Max. power voltage (V_{mp})	6 V	–
Seebeck coefficient, α		
PbTe (*n*-type)	$-225\ \mu V\ K^{-1}$	[13]
PbTe (*p*-type)	$+287\ \mu V\ K^{-1}$	[13]
Thermal conductivity, κ		
PbTe (*n*-type)	$2.07\ W\ m^{-1}\ K^{-1}$	Deduced from [13]
PbTe (*p*-type)	$1.448\ W\ m^{-1}\ K^{-1}$	[14]
Electrical resistivity, ρ		
PbTe (*n*-type)	$1.818 \times 10^{-5}\ \Omega\ m$	[13]
PbTe (*p*-type)	$2.56 \times 10^{-5}\ \Omega\ m$	[13]
Scale sun factor, CF	$1000\ W\ m^{-2}$	–

Table 2
Bismuth telluride (Bi_2Te_3) TE material particulars.

Parameter	Value (units)	Reference(s)
Peak TEG power (W_{mp})	3 W	–
Max. power voltage (V_{mp})	5 V	–
Seebeck coefficient, α		
Bi_2Te_3 (*n*-type)	$-250\ \mu V\ K^{-1}$	[15]
Bi_2Te_3 (*p*-type)	$+250\ \mu V\ K^{-1}$	[15]
Thermal conductivity, κ		
Bi_2Te_3 (*n*-type)	$1.359\ W\ m^{-1}\ K^{-1}$	Calc. from [15,16]
Bi_2Te_3 (*p*-type)	$1.736\ W\ m^{-1}\ K^{-1}$	Calc. from [16]
Electrical resistivity, ρ		
Bi_2Te_3 (*n*-type)	$2 \times 10^{-5}\ \Omega\ m$	[16]
Bi_2Te_3 (*p*-type)	$2 \times 10^{-5}\ \Omega\ m$	[16]
Scale sun factor, CF	$1000\ W\ m^{-2}$	–

under the same operating conditions. To facilitate our analysis, a design methodology was developed based on the principles of thermoelectricity [11], heat transfer, and the electrical and thermal characteristics of the device, the electrical load, the heat sink and the heat exchanger.

As depicted in Fig. 1, the segmented thermoelectric generator consists of a pair of *p*- and *n*-type Bi_2Te_3–PbTe thermoelements joined thermally in parallel and electrically in series. Thermal energy dissipation of the TEGs is achieved using active cooling with water as the cooling medium. Section 3.2.1.2 outlines the heat sink design methodology. The Seebeck coefficient of the *n*-type and *p*-type PbTe TE segments, clustered in Table 1, corresponded to doping levels of 0.03 mol% lead (II) iodide (PbI_2) and 0.3 atm.% sodium (Na), respectively. In the case of *n*- and *p*-type Bi_2Te_3 the α values, which appear in Table 2, refer to an electrical conductivity (σ) of $5 \times 10^4\ \Omega^{-1}\ m^{-1}$.

Using Fresnel optics it is possible to concentrate photons on the top plate of the TEG and raise the heat source temperature (T_H) to 623 K. Discrete *p*- and *n*-type TEG legs are electrically and thermally connected, on top of the TEG, using a copper plate, while a heat exchanger on the lower side of the system facilitates thermal energy dissipation. In contrast to natural convective heat dissipation, forced cooling, as explained in Section 3.2.1, could be employed to attain more effective thermal energy discharge at the heat sink. System particulars are presented in Tables 1 and 2.

3. Design methodology for segmented TEGs

3.1. Analytical model

First order approximations, based on simple equations, are often used to arrive to approximate design characteristics of TEGs before proceeding into more rigorous mathematical methods, such as computational modeling, and finally experimental fabrication. Hence, reliable, versatile and time efficient design methodologies are vital to the progress of high performance TEGs. Motivated by the latter need, in this work the formulation of a practical design methodology for segmented TEGs is presented.

Collectively, the TEG is to produce a peak power (P_{mp}) of 8 W, at a maximum power-voltage (V_{mp}) of 11 V. Because the TEG could be powered by concentrated solar thermal energy, system efficiency is investigated between a peak temperature of 622.8 K and an ambient temperature of 298.2 K. Maximum allowable current density (J_{max}) was set to $100\ A\ cm^{-2}$ [11] while the TEG open-circuit voltage (V_{oc}) was obtained by summing the Seebeck coefficients (α) of the constituent *p*- and *n*-type materials over the temperature gradient of interest

$$\Delta V_{oc} = \int_{T_C}^{T_H} [\alpha_{i,p}(T) - \alpha_{i,n}(T)]dT \tag{2}$$

where *i* is the material of interest for the *p*- and *n*-type materials, and T_H and T_C are the source and sink temperatures, respectively. An average α value over the temperature range of interest, denoted by $\bar{\alpha}$, is used for individual Bi_2Te_3 and PbTe materials and the segmented Bi_2Te_3–PbTe designs. Given that the TE elements are connected electrically in series, the (maximum power) current crossing each TEG unit can be determined from $P_{mp} = I_{mp} \times V_{mp}$. To determine the number of TEG units (n_{TEG}) needed to develop a total voltage of 11 V, the design methodology proposed by Da Rosa [11] was adapted with the introduction of appropriate modifications to reflect the peculiarities of the system. The maximum power voltage (V_{mp}) of the TEG system is obtained by summing the open circuit voltage drop across resistance *R*

$$n \cdot V_{oc} - n \cdot R \cdot I = V_{mp} \tag{3}$$

To deduce the number of TEG pairs (n_{TEG}), the TEG resistance (R) needs to be determined first. For peak efficiency, the load resistance, R_L, is given by

$$R_L = m \cdot n_{TEG} \cdot R \tag{4}$$

where $m = \sqrt{1 + \langle T \rangle \cdot Z}$ and $\langle T \rangle = (T_H + T_C)/2$. Furthermore, the device figure of merit (Z) is

$$Z = \frac{\alpha^2}{\Lambda \cdot R} \tag{5}$$

where Λ and R are the thermal conductance and the electrical resistance, respectively. The product $\Lambda \cdot R$ is obtained from

$$\Lambda \cdot R = \left(\sqrt{\kappa_i \cdot \rho_i} + \sqrt{\kappa_j \cdot \rho_j}\right)^2 \tag{6}$$

where *i* and *j* denote the materials of interest and ρ their electrical resistivity. Once Z is found, the total number of TEG pairs can also be obtained at the corresponding thermal gradient of interest. Conductive heat transfer (P_L) through the TEG is given by $P_L = \Lambda \cdot (T_H - T_C)$. Under electrical loading the thermal power supplied to the TEG by the heat source is

$$P_H = P_L + \alpha \cdot T_H \cdot I_i - \frac{1}{2} \cdot R_i \cdot I_i^2 \tag{7}$$

where I is the current of the TE material of interest denoted by *i*. Considering the thermal power under load (P_L) and no load (P_H) conditions, the efficiency of single-material Bi_2Te_3 and PbTe thermoelements can be determined from

$$\eta = \frac{P_L}{P_H} \tag{8}$$

The average Seebeck TEG design efficiency ($\bar{\eta}$) is obtained from the mean Seebeck coefficient ($\bar{\alpha}$), in turn, derived from the average total Seebeck values of the Bi_2Te_3 and PbTe materials

$$\bar{\eta} = \frac{\overline{P}_L}{\overline{P}_H} \tag{9}$$

Finally, the collective TEG design efficiency ($\tilde{\eta}$) is defined by summing the individual power developed by each of the constituent Bi_2Te_3 and PbTe thermoelectric elements based upon their total Seebeck coefficients

$$\tilde{\eta} = \frac{\sum P_{L_{i,j}}}{\sum P_{H_{i,j}}} \tag{10}$$

where subscripts i and j are the thermal power generated by the Bi_2Te_3 and PbTe thermoelectric materials, respectively.

One of the most effective and yet difficult ways to improve the efficiency of a TEG is to increase the device figure of merit, Z (Eq. (5)). Besides selecting TE materials with the largest possible z values, the geometry of the TE can help improve performance by decreasing the magnitude of the denominator ($\Lambda \cdot R$) (Eq. (6)). It turns out that there is a specific geometry, in terms of the TEG length and cross-sectional area, which minimizes $\Lambda \cdot R$ [11]

$$\frac{\ell_i \cdot A_j}{\ell_j \cdot A_i} = \left(\frac{\kappa_i \cdot \rho_j}{\kappa_j \cdot \rho_i}\right)^{1/2} \tag{11}$$

where ℓ is the length, A the cross-sectional area, and i and j are the p- and n-type TEG materials, respectively. Assuming that the TEG arms have the same overall length and experience a maximum current density (J_{max}) of 100 A cm^{-2}, A_i and A_j can be determined. Considering the resistance of individual thermoelements, one can obtain the length of the TE pairs using

$$R = \rho_i \cdot \frac{\ell}{A_i} + \rho_j \cdot \frac{\ell}{A_j} \tag{12}$$

In the sequel, the performance of individual Bi_2Te_3 and PbTe materials and the segmented Bi_2Te_3–PbTe designs are presented. Optimum system performance was obtained in the context of the TEG and load electrical resistance ratio and thermal TEG to heat sink and exchanger resistance ratio. Moreover, the optimum geometry for each TEG configuration was determined. Hereafter, the computational model is presented and the integration of results between the analytical and the computational models is outlined.

3.2. Computational Bi_2Te_3–PbTe TEG Model

Computational modeling, through the solution of partial differential equations (PDEs), generates insight otherwise unfathomable by experimental means. The temperature distribution and Direct Current (DC) conduction across the thermoelements which also govern the TEG efficiency are prominent examples. For segmented TEGs, of particular interest is the temperature gradient across each TE material which is dictated by the material's boundary conditions. Knowledge of the temperature at the Bi_2Te_3–PbTe interface can be used as input in the analytical model to derive the efficiency and the physical dimensions of the TEG configurations [17]. Joule heating and the Peltier and Seebeck effects were also implemented in the computational model. Fluid flow in the heat exchanger conduit, as shown in Fig. 2, was governed by the solution of the continuity and the Navier–Stokes equations. Table 3 presents the physical properties of the solid and liquid media comprising the computational model.

Fig. 2 shows the computational mesh used to trace the temperature variations across each TE material. The computational domain of the TEG model was discretized using structured conforming meshes mainly owing to the relatively simple geometry of the TEG design and the higher accuracy permitted by a structured, versus an unstructured, grid. The computational model presented in this work was developed using the multi-physics CFD-ACE + platform (ESI, Paris, France) [18]. A steady state time dependence was adopted for the solution of the governing equations.

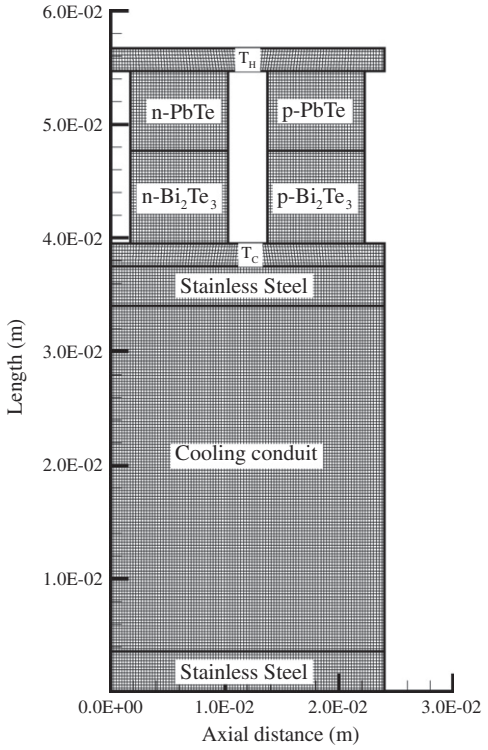

Fig. 2. The TEG-heat exchanger computational mesh for Bi_2Te_3–PbTe. The mesh consists of nine distinct computational zones with a total of 39,069 structured cells.

Table 3
Bi_2Te_3–PbTe computational model particulars.

Parameter (units)	Value	Reference(s)
Mass-density, ρ_m (kg m^{-3})		
Bi_2Te_3 (p- and n-type)	7740	[19]
PbTe (p- and n-type)	8160	[19]
Copper (Cu)	8960	[19]
Stainless steel 310	7782	[19]
Water (H_2O)	997	[19]
Specific heat capacity, C_p (J kg^{-1} K^{-1})		
Bi_2Te_3 (p- and n-type)	186	[20]
PbTe (p- and n-type)	155	[13]
Copper	385	[19]
Stainless steel 310	512	[19]
Water	4181	[19]
Thermal conductivity, κ (W m^{-1} K^{-1})		
Copper	401	[19]
Stainless Steel 310	14.99	[19]
Water	0.607	[19]
Dynamic viscosity, μ (kg m^{-1} s^{-1})		
Water	8.94×10^{-4}	[21]

3.2.1. Governing equations and boundary conditions

3.2.1.1. Heat transfer. Heat flux in the solid domain was traced through heat conduction while thermal energy transfer, in the cooling fluid, was governed by the numerical solution of the two-dimensional (2D) *total enthalpy equation* [22]

$$\frac{\partial(uh_0)}{\partial x} + \frac{\partial(vh_0)}{\partial y} = \kappa\left(\frac{\partial^2 T}{\partial x^2} + \frac{\partial^2 T}{\partial y^2}\right) + \left(\frac{\partial(u\tau_{xx})}{\partial x} + \frac{\partial(u\tau_{yx})}{\partial y} + \frac{\partial(v\tau_{xy})}{\partial x} + \frac{\partial(v\tau_{yy})}{\partial y}\right) \tag{13}$$

where $h_0 = i + p/\rho_m + \frac{1}{2}\cdot(u^2 + v^2)$ is the total enthalpy, p the static pressure, i the internal energy, and $\tau_{\imath,\jmath}$ is the viscous stress with i and j being the stress components acting on the $\jmath$-direction on a surface normal to direction $\imath$.

3.2.1.2. Heat exchanger. Establishing a high temperature gradient across the TEG calls for the use of an effective heat sink capable of handling a large thermal flux. For this purpose we have investigated both passive and active cooling. Owing to the high thermal flux a heat exchanger needs to dissipate, natural convective cooling – due to the large length of the cooling fins – becomes impractical.

Energy balance calculations revealed that heat dissipation can be efficiently accomplished using forced cooling with water as the working medium. For the sake of simplicity the length of the conduit, shown in Fig. 2, was assumed to match the same axial span as the thermal bridge connecting the two TEG arms. Flow in the conduit, in Cartesian coordinates, is governed by the 2D *continuity* and the *Navier–Stokes* equations for an incompressible Newtonian fluid. Considering that the mass–density (ρ_m) of the working medium does not vary with time and space, the 2D equations of flow with constant viscosity (μ) at a horizontal pipe orientation, ignoring gravity, reduce to [23]

$$\frac{\partial u}{\partial x}+\frac{\partial v}{\partial y}=0 \tag{14}$$

(x direction)

$$\rho_m\left(u\frac{\partial u}{\partial x}+v\frac{\partial u}{\partial y}\right)=-\frac{\partial p}{\partial x}+\mu\left(\frac{\partial^2 u}{\partial x^2}+\frac{\partial^2 u}{\partial y^2}\right) \tag{15a}$$

(y direction)

$$\rho_m\left(u\frac{\partial v}{\partial x}+v\frac{\partial v}{\partial y}\right)=-\frac{\partial p}{\partial y}+\mu\left(\frac{\partial^2 v}{\partial x^2}+\frac{\partial^2 v}{\partial y^2}\right) \tag{15b}$$

3.2.1.3. Electric, thermal and thermoelectric effects. Direct current conduction in the TE model was implemented through the numerical solution of Laplace's equation of the electric potential (ϕ). The two-dimensional Laplace's equation is

$$\underbrace{\sigma\left(\frac{\partial^2\phi}{\partial x^2}+\frac{\partial^2\phi}{\partial x^2}\right)}_{\phi^*}=0 \tag{16}$$

where σ is the electrical conductivity. Subsequently, the electric field (E) is determined from the 2D vector field

$$E=-\underbrace{\left(\frac{\partial\phi}{\partial x}\hat{\imath}+\frac{\partial\phi}{\partial y}\hat{\jmath}\right)}_{\epsilon^*} \tag{17}$$

Considering the Seebeck effect (α), Eq. (16) assumes the form

$$\phi^*=\alpha\cdot\sigma\left(\frac{\partial^2 T}{\partial x^2}+\frac{\partial^2 T}{\partial^2 y}\right) \tag{18}$$

Similarly, factoring in the thermoelectric phenomenon the new electric field, based on Eq. (17), is

$$E=-\epsilon^*+\alpha\left(\frac{\partial T}{\partial x}\hat{\imath}+\frac{\partial T}{\partial y}\hat{\jmath}\right) \tag{19}$$

Joule heating emanating from the thermal energy generated in a conductor, due to current flow, was modeled as a heat source [18]

$$H_T=\sigma\cdot\epsilon^{*2} \tag{20}$$

Finally, the Peltier power (P_s) implemented at the interface between two materials with thermoelectric properties is obtained from

$$P_s=\alpha\cdot T\cdot I \tag{21}$$

where I is the electric current.

3.2.1.4. Boundary conditions. For simplicity the top copper surface of the TEG was kept isothermal to 623 K throughout the simulations. The rest sides of the model were set adiabatic permitting thus only heat flux through the TEG elements to the cooling conduit – the latter of which serves as the heat sink (Fig. 2). Water entering the conduit, at the left side, was assumed to possess a uniform velocity of 0.1 m s^{-1} at a constant temperature of 298 K. Assuming a pipe with smooth internal surface, the low inlet velocity of water generated a laminar flow (Reynolds number, Re = 3,390). Based on this laminar flow we assumed that the entrance length of the pipe does exert an appreciable effect on convective heat dissipation. Therefore, we did not consider a longer length pipe section necessary for establishing a fully developed flow.

Current density at the top electrical bridge, connecting the two TEG elements, was set to 100 A cm^{-2} while the bottom ends of the TEG legs were electrically grounded (ϕ = 0). No current was assumed to escape the rest sides of the TEG and the bottom conducting bridge. Hence the bottom electrical plate and the cooling pipe were kept in electrical isolation from the rest TEG system.

3.2.2. Grid dependence study

A grid (in) dependence study serves to assess the sensitivity of the numerical solution to parameters, such as, the type and number of computational cells. Moreover, it offers a first indication as to the self-consistency of the modeling results. Valuable information can also be extracted regarding the trade-offs between the accuracy and reliability of results, computational expense, and time.

To raise confidence in the results of the TEG system, the temperature distribution of three meshes consisting of 19,852 cells (Grid A), 39,069 cells (Grid B) and 83,347 cells (Grid C) were compared. Temperature evolution was traced at the axial center of the n- and p-type rods at the Bi_2Te_3–PbTe junctions. Converged temperature results, at the interface of the n- and p-type materials, exhibited a difference of less than 1% for the same time period.

As the number of cells increased from Grids A to B to C the difference in their mean interface temperatures ($\overline{T}_{Inter}$) shrank. Grid B,

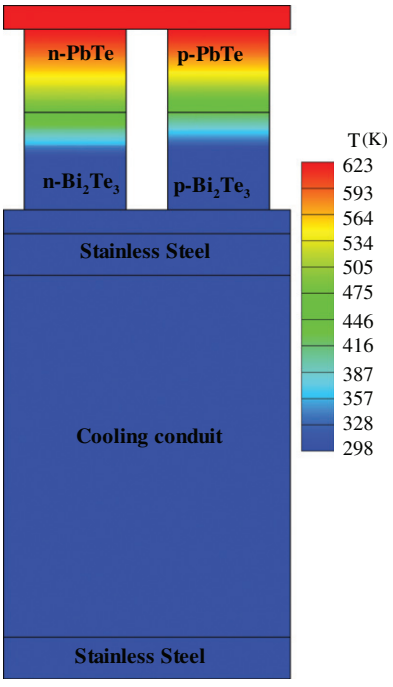

Fig. 3. Temperature distribution in the Bi_2Te_3–PbTe segmented TEG, at t = 213 min. The heat source (top) temperature (T_H) is 623 K while the heat sink (bottom) temperature (T_C) is 298 K. Minor temperature discrepancies between the n-type (left) and the p-type (right) TE legs arise from different material properties.

with 39,069, was selected as the most suitable model because it exhibited the best balance in terms of accuracy and computational time. With only a minute $\overline{T}_{Inter}$ difference of 3.5×10^{-2}% it reached convergence in 213 min versus 351 min for Grid C. Coarser grid A was rejected because it yielded a $\overline{T}_{Inter}$ deviation of 0.88% and 0.92% from Grids B and C, respectively. Section 3.2.3 outlines the process of obtaining $\overline{T}_{Inter}$.

3.2.3. Computational Bi_2Te_3–PbTe TEG model results

Numerical solution of the *energy equation* (13) in the computational domain (Fig. 2) revealed a slight temperature discrepancy between the *p*- and *n*-type interfaces of the Bi_2Te_3 and PbTe TE materials, as depicted in Fig. 3. To avoid undue complexity analytical calculations, as outlined in Section 4.2, are based on $\overline{T}_{Inter}$ obtained from the computational model. Variations in temperature between the two TEG legs emanate from differences in the values of the physical properties of the thermoelectric Bi_2Te_3 and PbTe materials, are shown in Table 3.

4. Results and discussion

4.1. Load-TEG electrical resistance matching

To evaluate the thermoelectric compatibility between PbTe and Bi_2Te_3, the compatibility factor (Eq. (1)) was used. If the difference in $\dot{s}$ values between two joined materials is less than a factor of two, the collective maximum efficiency does not deteriorate with segmentation [2]. A temperature gradient of 153.2 K across Bi_2Te_3, obtained from the computational model, yields a mean $\dot{s}$ value of 1.89 V^{-1}. Lead telluride, within the temperature range of operation (ΔT = 171.4 K), generates a mean $\dot{s}$ of 1.602 V^{-1}. Comparing the latter two $\dot{s}$ values reveals very good thermoelectric matching for Bi_2Te_3 and PbTe. Interconnected Bi_2Te_3 and PbTe TE elements including the copper bridges between the TE legs increase the overall electrical resistance of the TEG system. However, for small contact resistances (R_C) in relation to R_{TEG}, such that $R_C \ll R_{TEG}$, results (not included here) have shown that the contact resistance does not appreciably adversely affect the efficiency of the Bi_2Te_3, PbTe, Bi_2Te_3–PbTe ($\bar{\alpha}$), Bi_2Te_3–PbTe ($\tilde{\alpha}$) design configurations.

A thermoelectric generator produces maximum power output (P_{max}) when the TEG electrical resistance (R_{TEG}) is the same as the load electrical resistance (R_L); the dimensionless ratio of which is, often, denoted by $m = R_L/R_{TEG}$. Eq. (4) offers an alternative way of deriving m but not in terms of system optimization. Analyzing the relationship between R_L and R_{TEG} helps to quantify the optimum TEG (power) performance. In this context, there exists a single optimum m_{opt} value, usually $m_{opt} > 1$, at which the TEG yields the same power output but with a higher load electrical resistance. To simplify the procedure of determining m_{opt} we have developed a performance metric based on the rate of change of a material's efficiency as a function of the material's working temperature gradient ($\beta = \eta/\Delta T$).

As depicted in Fig. 4, Bi_2Te_3 with a β_{max} of 4.57×10^{-2} K^{-1} performs better than PbTe which reaches a β_{max} of 1.86×10^{-2} K^{-1}. Note that β_{max} defines the optimum m value (m_{opt}). When the average α value is considered for the segmented Bi_2Te_3–PbTe ($\bar{\alpha}$) TEG, β_{max} reaches a peak value of 5.67×10^{-2} K^{-1} compared to 2.82×10^{-2} K^{-1} for Bi_2Te_3–PbTe ($\tilde{\alpha}$). In terms of m, the optimum value of 1.545 is obtained in the case of the segmented Bi_2Te_3–PbTe ($\tilde{\alpha}$) with the TEG efficiency calculated on the performance of each individual material segment. As expected, the maximum (β_{max}) value of Bi_2Te_3–PbTe ($\tilde{\alpha}$) of 2.82×10^{-2} K^{-1} resides between the β_{max} values of Bi_2Te_3 and PbTe and favorably sustains a higher m value of 1.545. The aberrant β_{max} value of Bi_2Te_3–PbTe ($\bar{\alpha}$) is attributed to the normalization of α.

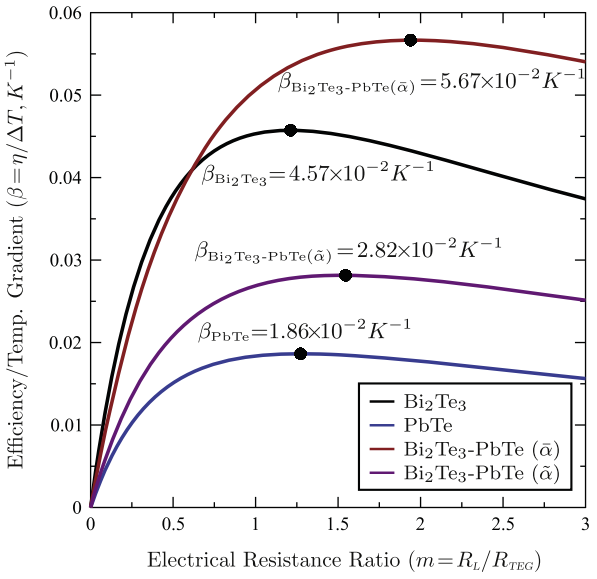

Fig. 4. Ratio of load (R_L) to TEG (R_{TEG}) electrical resistance as a function of the TEG temperature-dependent performance. Solid black circles denote m_{opt}, at the maximum β value, for each material or design configuration. The average and the collective Seebeck coefficient cases are denoted by $\bar{\alpha}$ and $\tilde{\alpha}$, respectively.

4.2. Integration of the analytical and computational models

Due to the interdependency between the TEG arms' length (ℓ) and the Bi_2Te_3–PbTe interface temperature (T_{Inter}), an iterative process was adopted to determine the latter parameters. Initially, the boundary condition temperatures T_H, T_C, and T_{Inter} were assumed to be 623 K, 298 K, and 475 K, respectively. Following the procedure outlined in Subsection 3.1 the efficiency and geometry of the TEG configurations were determined. The algorithm for obtaining the boundary condition temperatures T_H, T_C, and the mean Bi_2Te_3–PbTe interface temperature ($\overline{T}_{Inter}$) is based on an iterative procedure presented in Fig. 5.

4.3. TEG-heat sink thermal resistance matching

As a prerequisite for achieving the maximum TEG power, the TEG thermal resistance and the heat sink and heat source thermal resistance should match [1,24]. To investigate this assertion, the performance of the four design configurations (Bi_2Te_3, PbTe, Bi_2Te_3–PbTe ($\bar{\alpha}$), Bi_2Te_3–PbTe ($\tilde{\alpha}$)) was determined. For this purpose the TEG thermal resistance (Θ_{TEG}) to the heat source and heat exchanger thermal resistance (Θ_{Hx}), denoted by $n = \Theta_{TEG}/\Theta_{Hx}$, was used. Thermal resistance was implemented using $\Theta_{TEG_{ij}} = \ell_{TEG_{ij}}/(\kappa_{TEG_{ij}} \cdot A_{TEG_{ij}})$ where i and j refer to the *n*- and *p*-type materials of Bi_2Te_3 and PbTe. The latter equation was used to determine the thermal power under no-load (P_H) and load (P_L) conditions, for a range of n values, which defines the efficiency of the Bi_2Te_3–PbTe system (Eq. (8)). Contacts between the TE elements were assumed to be ideal therefore not negatively affecting the thermal performance of the TEG configurations examined herein. Normalized changes in efficiency (η) were used to identify the thermal resistance matching point between Θ_{TEG} and Θ_{Hx} which produced the peak TEG performance, that is, $\eta = 1$, as shown in Fig. 6.

Examining the trend of matching Θ_{TEG} and Θ_{Hx}, as depicted in Fig. 6, it becomes apparent that a correlation exists between thermal resistance and the temperature gradient (ΔT) within which each design configuration operates. Thermal matching ($\Theta_{TEG} = \Theta_{Hx}$) for Bi_2Te_3 occurs at 5.06 K W^{-1} for ΔT = 153.2 K. For PbTe, when ΔT increases to 171.4 K, $\Theta_{TEG} = \Theta_{Hx}$ reduces to 4 K W^{-1}. Notably, Bi_2Te_3–PbTe ($\bar{\alpha}$) and Bi_2Te_3–PbTe ($\tilde{\alpha}$) register the

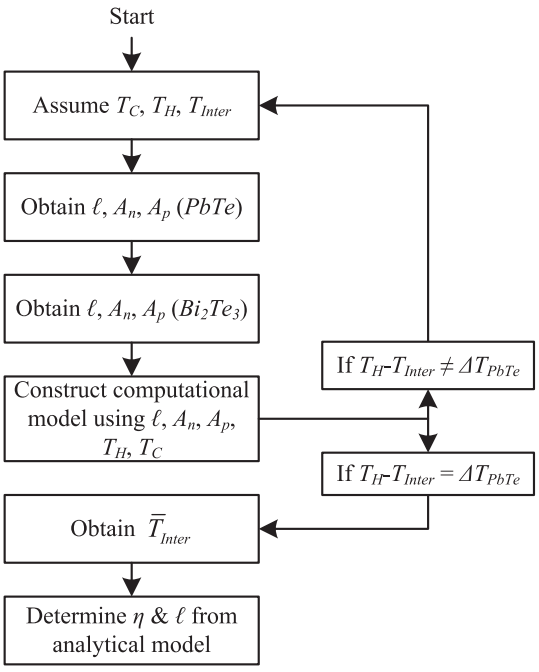

Fig. 5. Iterative process of determining the efficiency and geometry of segmented Bi_2Te_3–PbTe TEGs based upon the computational and analytical models.

maximum thermal resistance matching point ($\Theta_{TEG} = \Theta_{Hx}$) of 12.62 K W^{-1} when ΔT increases to 324.6 K.

Compared to Bi_2Te_3 and PbTe, the average ($\bar{\alpha}$) and collective ($\tilde{\alpha}$) Bi_2Te_3–PbTe designs exhibit a considerably higher (60–68%) source and sink thermal resistance matching ($\Theta_{TEG} = \Theta_{Hx}$). Apparently, matching the thermal resistance of the heat source and heat exchanger to the TEG thermal resistance is another necessary step towards optimizing the TEG performance.

4.4. Segmented and average seebeck coefficient Bi_2Te_3–PbTe TEGs

A simplified way to derive the efficiency of a segmented TEG is to average the Seebeck coefficient (α) values of the constituent

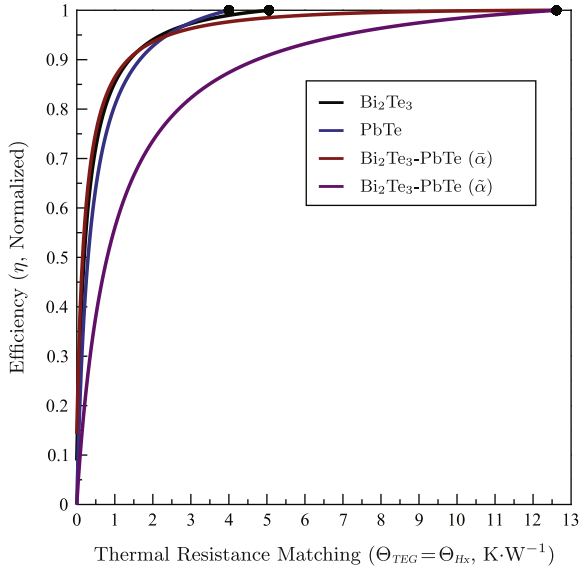

Fig. 6. Normalized changes in efficiency as a function of the thermal resistance matching between the TEG (Θ_{TEG}) and the heat source and heat exchanger (Θ_{Hx}). Maximum TEG system performance is attained when Θ_{Hx} matches Θ_{TEG}, i.e., $\eta = 1$.

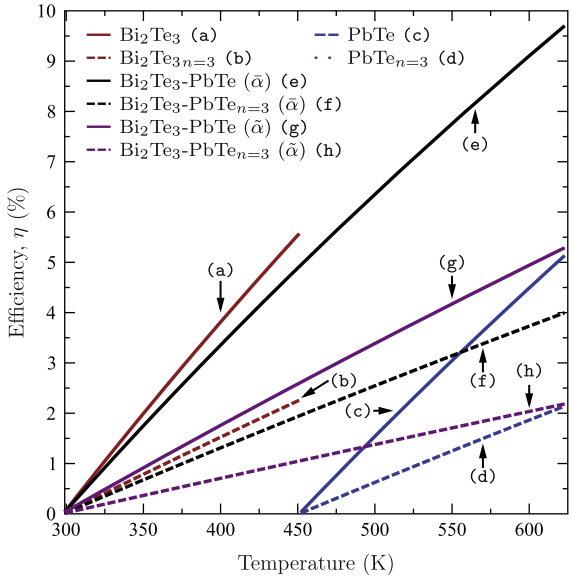

Fig. 7. Efficiency of individual Bi_2Te_3 and PbTe TEG materials and mean ($\bar{\alpha}$) and collective ($\tilde{\alpha}$) segmented TEGs. The reduced material efficiencies for a given configuration indicate the TEG to heat source and heat exchanger thermal resistance ratio $n = \Theta_{TEG}/\Theta_{Hx} = 3$.

elements over the TEG operating temperature range. Using the average Seebeck coefficient (Bi_2Te_3–PbTe), V_{oc} can be obtained for $\Delta T = 324.6$ K. Subsequently, m (Bi_2Te_3–PbTe) and n (Bi_2Te_3–PbTe) can be determined from the methodology outlined in Subsection 3.1. Eventually, the full load thermal power (P_H) of the TEG, upon which the TEG efficiency (η) is based, is derived. The efficiency of the segmented TEGs is obtained by considering the full thermal power produced by the individual thermoelements of Bi_2Te_3 and PbTe over their respective temperature regime.

Averaging the Seebeck coefficient (α) values of Bi_2Te_3 and PbTe within the entire temperature gradient of the TEG, of 324.6 K, appears to overestimate the Bi_2Te_3–PbTe peak efficiency (η, Fig. 7). However, when the efficiency of the segmented Bi_2Te_3–PbTe configuration is derived from the performance of the individual Bi_2Te_3 and PbTe materials, based on their corresponding α values, an η value of 5.29% was obtained (Bi_2Te_3–PbTe ($\tilde{\alpha}$), Fig. 7). The latter value is in very good agreement with other investigator's findings [1,7]. Matching the thermal resistance of the TEG to the thermal resistance of the heat source and the heat exchanger ($n = \Theta_{TEG}/\Theta_{Hx} = 1$), as depicted in Fig. 7, results in an increase maximum efficiency of 74.3% for Bi_2Te_3 ($\bar{\alpha}$) and 140.9% for Bi_2Te_3 ($\tilde{\alpha}$) relative to $n = 3$.

Results also indicate that for a given temperature gradient (ΔT) the magnitude of the Seebeck coefficient is the single most important parameter which governs efficiency. In other words, theoretical performance calculations largely reflect both the theoretical methodology and the accuracy of α values. Clearly, further progress should factor in the temperature dependent variation in α.

4.5. Geometry of the TE elements

The optimum TEG dimensions which maximize the TEG device figure of merit (and efficiency) are derived from Eq. (11). Results for Bi_2Te_3, PbTe, Bi_2Te_3–PbTe ($\bar{\alpha}$), and Bi_2Te_3–PbTe ($\tilde{\alpha}$) for the corresponding temperature gradient of interest and J_{max}, yield different TE lengths, as depicted in Fig. 8. Of particular interest is the more compact size of the segmented Bi_2Te_3–PbTe ($\tilde{\alpha}$) whose length measures 0.152 cm (or 4.6% shorter) in comparison to Bi_2Te_3–PbTe ($\bar{\alpha}$) which has a length of 0.159 cm. Results also suggest an

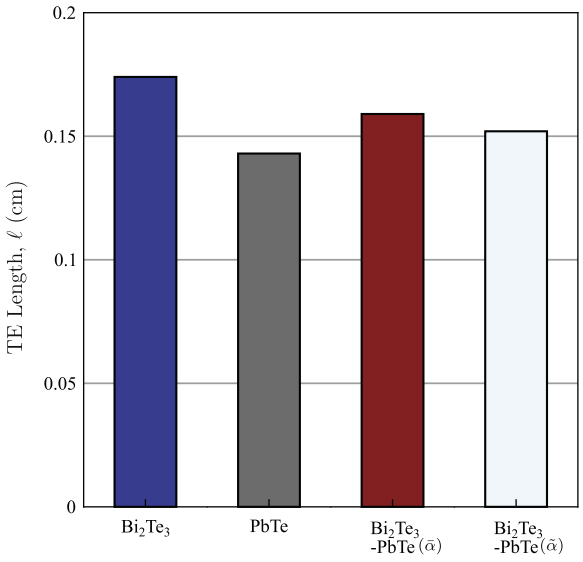

Fig. 8. Length of the thermoelement (TE) couples of the Bi_2Te_3 and PbTe materials and the average Bi_2Te_3–PbTe ($\bar{\alpha}$) and collective Bi_2Te_3–PbTe ($\tilde{\alpha}$) configurations.

inversely proportional correlation between the TEG arms' lengths and the maximum current density.

5. Conclusions

Confirming experimental measurements, analytical modeling results, augmented by computational simulations, of the maximum efficiency to temperature gradient ($\beta_{max} = \frac{\eta}{\Delta T}$) showed that the collective Seebeck coefficient Bi_2Te_3–PbTe ($\tilde{\alpha}$) design can support a higher electrical load in relation to the homogeneous Bi_2Te_3 and PbTe materials. Averaging the Seebeck coefficient in the case of Bi_2Te_3–PbTe ($\bar{\alpha}$) TEG overestimates β_{max}, at the highest m value, compared to the Bi_2Te_3, PbTe, and Bi_2Te_3–PbTe ($\tilde{\alpha}$) TEGs. Optimum TEG performance (η) in terms of matching the TEG to the heat source and heat exchanger thermal resistance ratio revealed that the thermal resistance of the segmented TEG system increases with the temperature gradient of the TEG. Matching Θ_{TEG} to Θ_{Hx} is a prerequisite for maximizing the TEG system efficiency and controlling the size of the heat exchanger which, in turn, governs the physical dimensions of the TEG. Actively cooled heat exchangers, as our results demonstrate, constitute an attractive option for high thermal energy density dissipation and compact TEGs.

Computational results provided exquisite details of the temperature distribution across the TEG legs which, in turn, helped raise the accuracy of the analytical results. In closing, the hybrid computational–analytical modeling approach achieves a very good level of accuracy as part of a time efficient framework.

Acknowledgments

This research was partially supported by the University of Cyprus. Financial support from the Department of Electrical and Computer Engineering, University of Cyprus, is also acknowledged. The authors want to express their gratitude to Prof. Yiannis Ventikos of the University of Oxford for his insight.

References

[1] Priya S, Inman DJ. Energy harvesting technologies. Boston (MA): Springer; 2009.
[2] Snyder GJ, Ursell TS. Thermoelectric efficiency and compatibility. Phys Rev Lett 2003;91:1483011–14.
[3] Snyder GJ. Application of the compatibility factor to the design of segmented and cascaded thermoelectric generators. Appl Phys Lett 2004;84:2436–8.
[4] Snyder GJ, Toberer ES. Complex thermoelectric materials. Nat Mater 2008;7:105–14.
[5] Astrain D, Vián JG, Martinez A, Rodriguez A. Study of the influence of heat exchangers' thermal resistances on a thermoelectric generation system. Energy 2010;35:602–10.
[6] Karri MA, Thacher EF, Helenbrook BT. Exhaust energy conversion by thermoelectric generator: two case studies. Energy Convers Manage 2011; 52:1596–611.
[7] Kraemer D, Poudel B, Feng H-P, Caylor JC, Yu B, Yan X, et al. High-performance flat-panel solar thermoelectric generators with high thermal concentration. Nat Mater 2011;10:532–8.
[8] Vikhor LN, Anatychuk LI. Generator modules of segmented thermoelements. Energy Convers Manage 2009;50:2366–72.
[9] El-Genk MS, Saber HH. High efficiency segmented thermoelectric unicouple for operation between 973 and 300 K. Energy Convers Manage 2003;44:1069–88.
[10] Kaltschmitt M, Streicher W, Wiese A. Renewable energy: technology. Economics and environment. New York: Springer; 2007.
[11] Da Rosa AV. Fundamentals of renewable energy processes. Amsterdam: Elsevier; 2009.
[12] Schilz J, Helmers L, Muller WE, Niino M. A local selection criterion for the composition of graded thermoelectric generators. J Appl Phys 1998;83: 1150–2.
[13] Dughaish ZH. Lead telluride as a thermoelectric material for thermoelectric power generation. Physica B 2002;322:205–23.
[14] Snyder GJ, Christensen M, Nishibori E, Caillat T, Iversen BB. Disordered zinc in Zn_4Sb_3 with phonon-glass and electron-crystal thermoelectric properties. Nat Mater 2004;3:458–63.
[15] Rowe DM. CRC handbook of thermoelectrics. Boca Raton (FL): CRC Press; 1995.
[16] Goldsmid HJ. Introduction to thermoelectricity. New York: Springer; 2010.
[17] Hadjistassou C, Kyriakides E, Georgiou J. Designing hybrid photovoltaic–thermoelectric energy systems. In: 3rd International conference on renewable energy sources & energy efficiency, Nicosia, Cyprus, May 19–20; 2011. p. 242–50. <http://www.mse.com.cy/energy/2011.pdf> [accessed 09.05.12].
[18] ESI, CFD-ACE+V2006 user manual, Paris, France; 2006.
[19] Lide DR. CRC handbook of chemistry and physics. 90th ed. Boca Raton: CRC Press; 2010.
[20] Wang H, Porter WD, Sharp J. Thermal conductivity measurements of bulk thermoelectric materials. In: Proceedings of 24th international conference on thermoelectrics 2005, Clemson, SC, USA. p. 91–4.
[21] Douglas JF. Fluid mechanics. England: Pearson/Prentice Hall; 2005.
[22] Versteeg HK, Malalasekera W. An introduction to computational fluid dynamics. New York: Pearson; 2007.
[23] Munson BR. Fundamentals of fluid mechanics. 6th ed. New York: John Wiley; 2009.
[24] Stevens JW. Optimal design of small ΔT thermoelectric generation systems. Energy Convers Manage 2001;42:709–20.